Detection and Discrimination of Land Mines in Ground-Penetrating Radar Based on Edge Histogram Descriptors and a Possibilistic K-Nearest Neighbor Classifier

Hichem Frigui, *Member, IEEE*, and Paul Gader, *Senior Member, IEEE*

***Abstract*—This paper describes an algorithm for land mine detection using sensor data generated by a ground-penetrating radar (GPR) system that uses edge histogram descriptors for feature extraction and a possibilistic K-nearest neighbors (K-NNs) rule for confidence assignment. The algorithm demonstrated the best performance among several high-performance algorithms in extensive testing on a large real-world datasets associated with the difficult problem of land mine detection. The superior performance of the algorithm is attributed to the use of the possibilistic K-NN algorithm, thereby providing important evidence supporting the use of possibilistic methods in real-world applications. The GPR produces a 3-D array of intensity values, representing a volume below the surface of the ground. First, a computationally inexpensive prescreening algorithm for anomaly detection is used to focus attention and identify candidate signatures that resemble mines. The identified regions of interest are processed further by a feature extraction algorithm to capture their salient features. We use translation-invariant features that are based on the local edge distribution of the 3-D GPR signatures. Specifically, each 3-D signature is divided into subsignatures, and the local edge distribution for each subsignature is represented by a histogram. Next, the training signatures are clustered to identify prototypes. The main idea is to identify few prototypes that can capture the variations of the signatures within each class. These variations could be due to different mine types, different soil conditions, different weather conditions, etc. Fuzzy memberships are assigned to these representatives to capture their degree of sharing among the mines and false alarm classes. Finally, a possibilistic K-NN-based rule is used to assign a confidence value to distinguish true detections from false alarms. The proposed algorithm is implemented and integrated within a complete land mine prototype system. It is trained, field-tested, evaluated, and compared using a large-scale cross-validation experiment that uses a diverse dataset acquired from four outdoor test sites at different geographic locations. This collection covers over 41 807 m^2 of ground and includes 1593 mine encounters.**

Manuscript received February 27, 2008; revised June 23, 2008; accepted August 16, 2008. First published September 3, 2008; current version published February 4, 2009. This work was supported in part by the National Science Foundation (NSF) under Award CBET-0730802 and Award CBET-0730484, by the Kentucky Science and Engineering Foundation under Grant KSEF-148-502-05-153, by the U.S. Army under Grant DAAB15-02-D-0003, by the Office of Naval Research under Award N00014-05-10788, and by an Army Research Office and U.S. Army Research Laboratory under Cooperative Agreement DAAD19-02-2-0012.

H. Frigui is with the Department of Computer Engineering and Computer Science, University of Louisville, Louisville, KY 40292 USA (e-mail: h.frigui@louisville.edu).

P. Gader is with the Department of Computer and Information Science and Engineering, University of Florida, Gainesville, FL 32611-6120 USA (e-mail: pgader@cise.ufl.edu).

Color versions of one or more of the figures in this paper are available online at http://ieeexplore.ieee.org.

Digital Object Identifier 10.1109/TFUZZ.2008.2005249

***Index Terms*—Edge histogram descriptor, feature-based discrimination, land mine detection, possibilistic K-nearest neighbor (K-NN).**

I. Introduction

DETECTION and removal of land mines is a serious problem affecting civilians and soldiers worldwide. *"These hidden killers are cheap to buy, easy to use, hard to detect, and difficult to remove"* [1]. They cost as little as $3 to make, but as much as $1000 to remove. The fact that more land mines are deployed in armed conflicts every year than are removed has caused over 80 countries around the world to be littered by more than 100 million buried land mines. Consequently, it is estimated that more than 26 000 people, mostly civilians, in a year are either killed or maimed by a land mine [1], [2]. Detection and removal of land mines is therefore a significant problem and has attracted several researchers in recent years [3]–[7]. The detection problem is compounded by the large variety of land mine types, differing soil conditions, temperature and weather conditions, and varying terrain, to name a few. Traditional fielded approaches use metal detectors. Unfortunately, many modern land mines are made of plastic and contain little or no metal.

A variety of sensors have been proposed or are under investigation for land mine detection [8]–[11]. The research problem for sensor data analysis is to determine how well signatures of land mines can be characterized and distinguished from other objects under the ground using returns from one or more sensors. Ground-penetrating radar (GPR) offers the promise of detecting land mines with little or no metal content. Unfortunately, land mine detection via GPR has been a difficult problem [8], [12], [13]. Although systems can achieve high detection rates, they have done so at the expense of high false alarm rates (FARs). The key challenge to mine detection technology lies in achieving a high rate of mine detection while maintaining low level of false alarms. The performance of a mine detection system is therefore commonly measured by a receiver operating characteristics (ROCs) curve that jointly specifies the rate of mine detection and level of false alarm.

Automated detection algorithms can generally be broken down into four phases: preprocessing, feature extraction, confidence assignment, and decision making. Preprocessing algorithms perform tasks such as normalization of the data, corrections for variations in height and speed, removal of stationary effects due to the system response, etc. Methods that have

been used to perform this task include wavelets and Kalman filters [14], [15], subspace methods and matching to polynomials [16], subtracting optimally shifted and scaled reference vectors [17], and inverse modeling [18]. Feature extraction algorithms reduce the preprocessed raw data to form a lower dimensional, salient set of measures that represent the data. Principal component (PC) transforms are a common tool to achieve this task [19], [20]. Other feature analysis approaches include wavelets [14], kernel methods [21], image processing methods of derivative feature extraction [22], curve analysis using Hough and Radon transforms [5], as well as model-based methods [23]. Confidence assignment algorithms can use methods such as Bayesian [5], hidden Markov models [22], [24], fuzzy logic [6], rules and order statistics [25], neural networks [26], support vector machines [27], or nearest neighbor (NN) classifiers [28], [29] to assign a confidence that a mine is present at a point. Decision-making algorithms often postprocess the data to remove spurious responses and use a set of confidence values produced by the confidence assignment algorithm to make a final mine/no-mine decision.

In this paper, we propose a feature-based algorithm for land mine detection in GPR data that use edge histogram descriptors (EHDs) for feature extraction and a possibilistic K-NN-based classifier for confidence assignment. First, an adaptive LMSs prescreener, proposed by Torrione *et al.* [30], is used to focus attention and identify regions with subsurface anomalies. Second, the identified candidates are processed further by our previously developed feature-based discrimination algorithm [28] to attempt to separate mine targets from naturally occurring clutter. Specifically, each 3-D signature is divided into subsignatures, and the local edge distribution for each subsignature is represented by a histogram. To generate the histogram, local edges are categorized into five types: vertical, horizontal, diagonal, antidiagonal, and nonedges. Third, a set of alarms with known ground truth is used to train the decision-making process. These alarms are clustered to identify few representatives. The main idea is to summarize the training data and identify few prototypes that can capture the variations of the signatures within each class. These variations could be due to different mine types, different soil conditions, different weather conditions, etc. Fuzzy memberships are assigned to the representatives to capture their degrees of sharing among the mine and clutter classes. Finally, a possibilistic K-NN-based rule, which is robust to noisy signatures, is proposed and used to assign a confidence value to distinguish true detections from false alarms.

The rest of this paper is organized as follows. Section II gives an overview of the GPR data and the preprocessing steps. Section III describes the different steps of the proposed edge-based detection system. Evaluation methods and experimental results are presented in Section IV, and concluding remarks are given in Section V.

II. Data Preprocessing and Prescreening

In this section, we present a brief description of the GPR data, the preprocessing steps, and the LMS prescreener. A more detailed description of these steps can be found in [25] and [30].

Fig. 1. NIITEK vehicle mounted GPR system.

A. GPR Data

The input data consist of a sequence of raw GPR signatures collected by an NIITEK, Inc., land mine detection system comprising a vehicle-mounted 51-channel GPR array (see Fig. 1) [31]. The NIITEK GPR collects 51 channels of data. Adjacent channels are spaced approximately 5 cm apart in the cross-track direction, and sequences (or scans) are taken at approximately 6 cm down-track intervals. The system uses a V dipole antenna that generates a wideband pulse ranging from 200 MHz to 7 GHz. Each A-scan, i.e., the measured waveform that is collected in one channel at one down-track position, contains 416 time samples at which the GPR signal return is recorded. Each sample corresponds to roughly 8 ps. We often refer to the time index as depth although, since the radar wave is traveling through different media, this index does not represent a uniform sampling of depth. Thus, we model an entire collection of input data as a 3-D matrix of sample values $S(z,x,y), z=1,\ldots,416;\ x=1,\ldots,51;\ y=1,\ldots,N_S$, where N_S is the total number of collected scans, and the indexes z, x, and y represent depth, cross-track position, and down-track positions, respectively. A collection of scans, forming a volume of data, is illustrated in Fig. 2.

Fig. 3 displays several B-scans (sequences of A-scans) both down-track (formed from a time sequence of A-scans from a single-sensor channel) and cross-track (formed from each channels response in a single sample). The surveyed object position is highlighted in each figure. The objects scanned are: 1) a high-metal-content antitank mine; 2) a low-metal-content antitank mine; and 3) a wood block.

B. Data Alignment and Time Gating

Preprocessing is an important step to enhance the mine signatures for detection. In the proposed system, first we identify the location of the ground bounce as the signal's peak and align the multiple signals with respect to their peaks. This alignment is necessary because the vehicle-mounted system cannot maintain the radar antenna at a fixed distance above the ground. Since

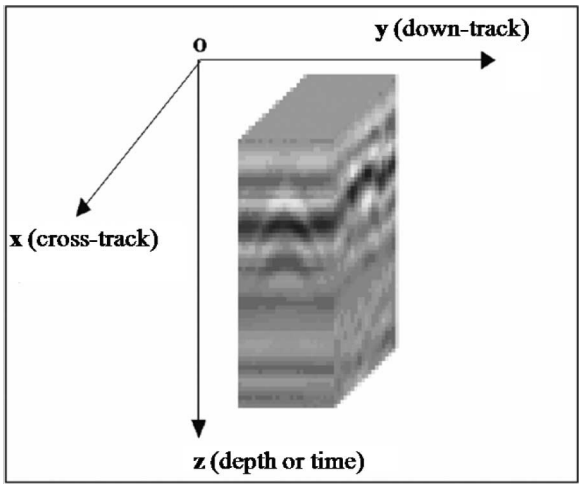

Fig. 2. Collection of few GPR scans.

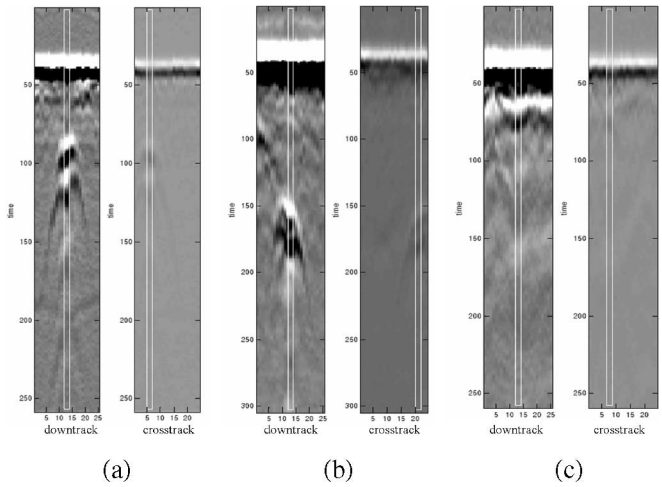

Fig. 3. NIITEK radar down-track and cross-track B-scans pairs for three alarms. (a) Metal mine. (b) Low-metal mine. (c) Wood block.

the system is looking for buried objects, the early time samples of each signal up to few samples beyond the ground bounce are discarded so that only data corresponding to regions below the ground surface are processed.

C. Anomaly Detection

Rather than exhaustively process each of the many discrete locations sampled by the GPR array, our system employs a prescreener to reduce the volume of data to be inspected. In particular, the prescreener identifies distinct alarms (points of interest) in the data and can be thought of as a conservative detection algorithm, i.e., a detector designed to provide a high probability of land mine detection at the expense of inclusion of many false alarms. False alarms arise as a result of radar signals that present a mine-like character. Such signals are generally said to be a result of clutter. The objective of the proposed feature-based detection algorithm is to discriminate between those prescreener alarms corresponding to land mines and those corresponding to clutter.

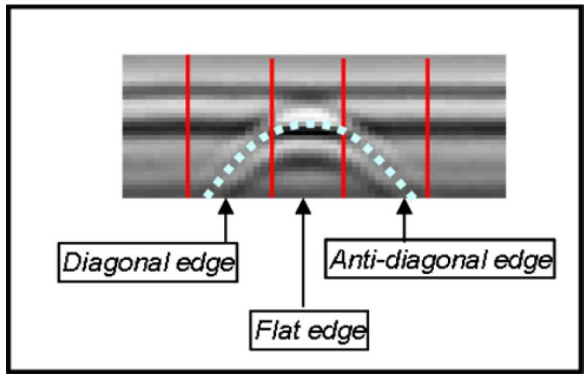

Fig. 4. Features of a mine signature.

In this paper, we report the results when the raw GPR data are preprocessed using the NUKEv6 prescreener developed at Duke University [30] and implemented in real time. This prescreener is an adaptation of the 2-D LMS algorithm that has been widely used [32]. In particular, it incorporates several pre- and postprocessing steps to maintain low FAR in the NIITEK GPR data. This prescreener is applied to each point in the cross-track, down-track plane, and produces a confidence value at each location indicating the likelihood that a mine is present. These confidence values are grouped spatially into components. The components that satisfy empirically predetermined conditions are considered as potential targets. Their cross-track x_s and down-track y_s positions of the connected component center are reported as alarm positions for further processing.

III. Edge-Based Land Mine Detection

Land mines (and other buried objects) appear in time-domain GPR as shapes that are similar to hyperbolas corrupted by clutter. Fig. 4 displays a hyperbolic curve superimposed on a very clear, preprocessed metal mine signature to illustrate the features of a typical mine signature. As can be seen, the edges and their spatial distribution constitute an important feature to characterize the mine signatures. Thus, the feature representation adopted by the proposed system is based on the degree to which edges occur and their relative orientations.

A. Edge Histogram Descriptor

In the following, we describe our feature extraction algorithm that captures the salient properties of the 3-D alarms in a compact and translation-invariant representation. This feature representation was first introduced in [28]. This approach, inspired by the MPEG-7 EHD [33], extracts edge histograms capturing the frequency of occurrence of edge orientations in the data associated with a ground position. The basic MPEG-7 EHD has undergone rigorous testing and development, and thus, represents one of the mature, generic, and efficient texture descriptors. For a generic image, the EHD represents the frequency and the directionality of the brightness changes in the image. Simple edge detector operators are used to identify edges and group them into five categories: vertical, horizontal, 45° diagonal, 135° antidiagonal, and isotropic (nonedges). The

EHD would include five bins corresponding to the aforementioned categories.

For our application, we adapt the EHD to capture the spatial distribution of the edges within a 3-D GPR data volume. To keep the computation simple, we still use 2-D edge operators, but we compute two types of edge histograms. The first one is obtained by fixing the cross-track dimension and extracting edges in the (depth, down-track) plane. The second edge histogram is obtained by fixing the down-track dimension and extracting edges in the (depth, cross-track) plane. Also, since vertical, horizontal, diagonal, and antidiagonal edges are the main orientations present in the mine signatures, we keep the five edge categories of the MPEG-7 EHD.

Let $S_{zy}^{(x)}$ be the xth plane of the 3-D signature $S(x, y, z)$. First, for each $S_{zy}^{(x)}$, we compute four categories of edge strengths: vertical, horizontal, 45° diagonal, and 135° antidiagonal. If the maximum of the edge strengths exceeds a certain preset threshold θ_G, the corresponding pixel is considered to be an edge pixel. Otherwise, it is considered a nonedge pixel. A global histogram that captures the frequency of the different edge orientations cannot take into account the relative position of the different edges. For instance, it cannot discriminate between mine signatures with a concave down hyperbolas and background signatures with a concave up hyperbolas. To overcome this limitation, each $S_{zy}^{(x)}$ image is vertically subdivided into seven overlapping subimages $S_{zy_i}^{(x)}, i = 1, \ldots, 7$. For each $S_{zy_i}^{(x)}$, a five-bin edge histogram $H_{zy_i}^{(x)}$ is computed. The bins correspond to the four edge categories and the nonedge pixels. The overlap is needed to make the subimages large enough to include sufficient edges, and reduce the sensitivity of the feature representation to the width and shift variations of the signatures.

The down-track component of the EHD or EHD^y is defined as the concatenation of the 7 five-bin histograms, i.e.

$$\text{EHD}^d(S_{xyz}) = [\overline{H}_{zy_1}\, \overline{H}_{zy_2}\, \overline{H}_{zy_3} \cdots \overline{H}_{zy_7}] \tag{1}$$

where $\overline{H}_{zy_i}$ is the cross-track average of the edge histograms of subimage $S_{zy_i}^{(x)}$ over N_C channels, i.e.

$$\overline{H}_{zy_1} = \frac{1}{N_C} \sum_{x=1}^{N_C} H_{zy_i}^{(x)}.$$

To compute the cross-track component of the EHD or EHD^x, we fix the scans and compute the four edge strengths on the $S_{zx}^{(y)}, y = 1, \ldots, N_S$ (depth, cross-track) planes. Since these planes do not have enough columns (typically <7) where the signature is present, they are not divided into subimages, and only one global histogram per plane H_{zx}^{y} is computed, i.e., EHD^x is computed as the down-track average of the edge histograms over N_S scans

$$\text{EHD}^x(S_{xyz}) = \frac{1}{N_S} \sum_{y=1}^{N_S} H_{zx}^{(y)}. \tag{2}$$

The EHD of each 3-D GPR alarm is a 40-D histogram that concatenates the down-track and cross-track EHD components,

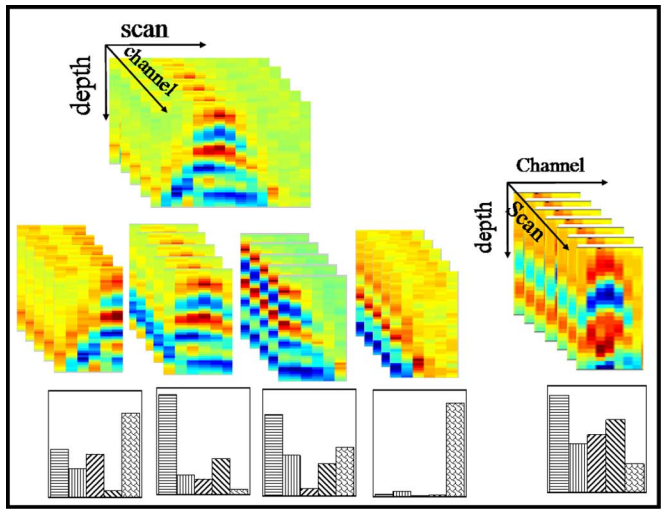

Fig. 5. Extraction of the EHD for a 3-D mine signature. For clarity, only four of the seven subimages in the (depth, down-track) plane are shown.

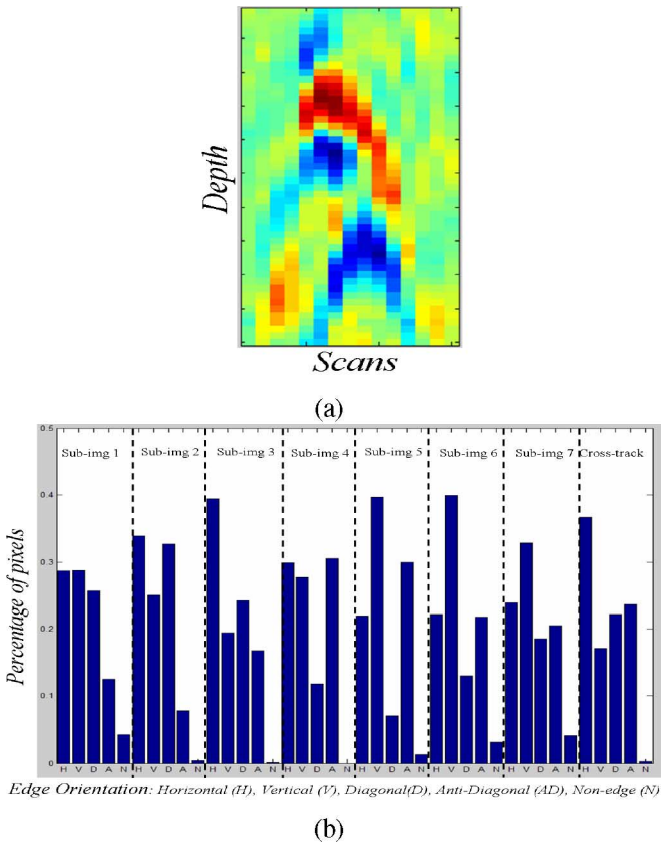

Fig. 6. EHD feature of a strong mine signature. (a) Mine signature in the (depth, down-track) plane. (b) Concatenated edge histograms extracted from the down-track component (seven subimages) and the cross-track component.

i.e.

$$\text{EHD}(S_{xyz}) = [\text{EHD}^y(S_{xyz})\ \ \text{EHD}^x(S_{xyz})]. \tag{3}$$

The extraction of the EHD is illustrated in Fig. 5.

Figs. 6 and 7 display the edge histogram feature for a strong mine and a false alarm identified by the prescreener due to its

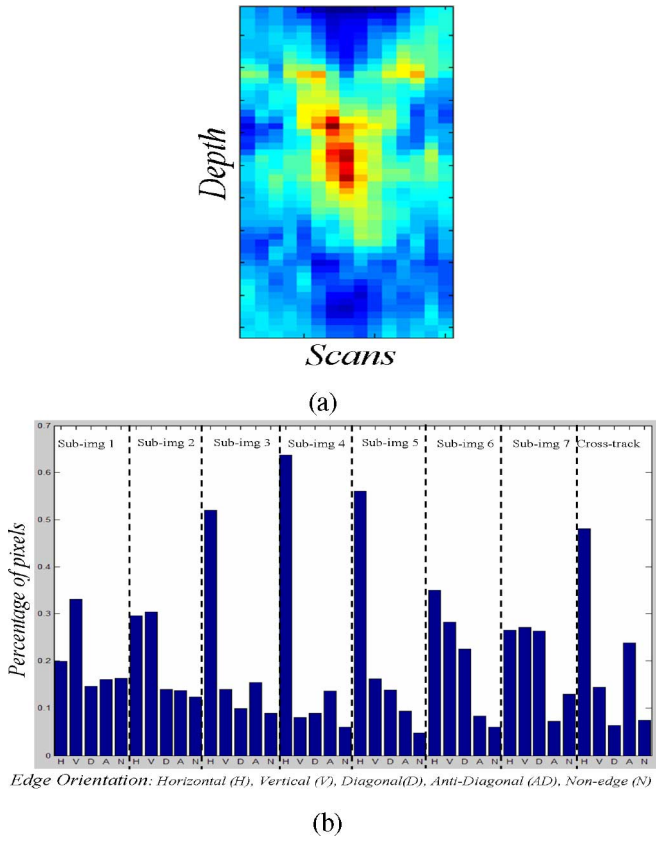

Fig. 7. EHD feature of a false alarm signature. (a) Alarm signature in the (depth, down-track) plane. (b) Concatenated edge histograms extracted from the down-track component (seven subimages) and the cross-track component.

high-energy contrast. As can be seen, the EHD of the mine signature can be characterized by a stronger response to the diagonal and antidiagonal edges. Moreover, the frequency of the diagonal edges is higher than the frequency of the antidiagonal edges on the left subimages (rising edge of the signature) and lower on the right subimages (falling edge). This feature is typical in mine signatures. The EHD of the false alarm, on the other hand, does not follow this pattern. The edges do not follow a specific structure, and the diagonal and antidiagonal edges are usually weaker.

B. K-NN Classifiers

The land mine detection problem could be formulated as a one-class problem (e.g., using methods proposed in [34]). However, extensive experiments have indicated that it is more effective to treat the problem as a two-class problem (mine and clutter), assign a confidence value to each class independently, and aggregate the two confidence values. Moreover, since the results of the proposed algorithm will eventually be fused with the results of other algorithms, generating confidence values for both classes can provide more information. In addition, the real-time constraint of the considered application and the need to produce results that are easily interpretable led us to choose a simple K-NN classifier. In the following, we first provide an overview of the crisp and fuzzy K-NN classifiers. Then, we describe our proposed possibilistic version of this classifier.

1) Crisp K-NN Classifier: The K-NN classification rule is a voting scheme that is widely used in pattern recognition and classification problems, such as face recognition [35], character recognition [36], and land mine detection [28]. K-NN classifiers are appealing because of their simplicity, ability to model non-parametric distributions, and theoretical optimality as the size of the training data goes to infinity. The conventional K-NN classification rule [37] assigns an input pattern to the class of the majority of its K-NNs, of known classification, according to a distance measure. Dudani [38] proposed a weighted K-NN rule where the NNs are weighted according to their proximity to the test pattern. Various other extensions and improvements have been proposed [39], [40].

2) Fuzzy K-NN Classifier: A common drawback of the crisp K-NN classification rule is that the K nearest training patterns are treated equally important in the confidence assignment of the test pattern. This may degrade the classifier's accuracy in regions where patterns from different classes overlap. Keller *et al.* [41] proposed using fuzzy concepts to overcome this limitation. Their algorithm, called fuzzy K-NN, assigns a fuzzy membership (in [0, 1]) to each training pattern rather than using a binary class membership. The memberships are assigned in [41] using

$$\tilde{\mu}^i(y) = \begin{cases} 0.51 + (\frac{n_i}{K}) \times 0.49, & \text{if } i = j \\ (\frac{n_i}{K}) \times 0.49, & \text{if } i \neq j \end{cases} \quad (4)$$

where n_i denotes the number of neighbors that belong to the ith class, i.e., $\sum_{i=1}^{C} n_i = K$, and j is the actual class label of sample y. The pattern's fuzzy membership $\tilde{\mu}^i(x)$ controls its contribution during the classification process.

During testing, the membership value of a test pattern x in class i is computed using

$$\mu^i(x) = \sum_{k=1}^{K} \tilde{\mu}^i(y_k) w(x, y_k) \quad (5)$$

where

$$w(x, y_k) = \frac{\left(1/\|x - y_k\|^{2/(m-1)}\right)}{\sum_{k=1}^{K} \left(1/\|x - y_k\|^{2/(m-1)}\right)}. \quad (6)$$

In other words, the confidence value assigned to a test pattern depends on the membership degrees of the K-NNs and their relative proximity.

3) Possibilistic K-NN Classifier: The standard K-NN, weighted K-NN, and fuzzy K-NN cannot discriminate between neighbors that are equally close and neighbors that are equally far away. For instance, for both scenarios illustrated in Fig. 8, these algorithms will assign the same confidence value to x in class 1. This is despite the fact that in Fig. 8(b), x is not similar to any training patterns from class 1. This problem may not be severe if the test data do not significantly deviate from the training data. However, in some applications, it is not possible to collect enough training samples to cover the entire domain. For instance, in land mine detection, it is not possible to collect false alarm signatures that cover all possible objects, all terrain types, all environment conditions, etc. In this case, the

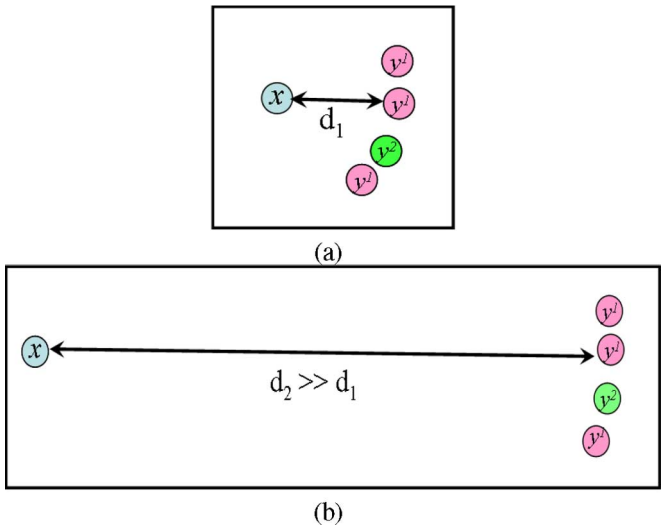

Fig. 8. Limitations of the K-NN, weighted K-NN, and fuzzy K-NN. (a) Typical test sample x with four close neighbors (three from class 1 and one from class 2). (b) Nontypical test sample where the closest four neighbors are far away. The three algorithms will assign a confidence value around 0.75 to x in class 1 for both cases.

confidence value assigned using the standard, weighted, or fuzzy K-NN to nontypical signatures are not reliable.

To overcome this limitation, we propose a possibilistic version of the fuzzy K-NN where the weights depend on the absolute distance of the test pattern from its K-NNs. In other words, instead of using weights as in (6) that sum to 1, we use possibilistic weights [42], [43] that relax this constraint. In particular, we use

$$w^p(x, y_k) = \frac{1}{1 + \left[\max\left(0, \|x - y_k\| - \eta_1/\eta_2\right)\right]^{2/(m-1)}} \quad (7)$$

where η_1 and η_2 are the constants that are estimated from the training data (as will be described in Section IV-B). In (7), $m \in (1, \infty)$ is a constant that controls the fuzziness of the weight function. In the experiments reported in this paper, we set m to 2. Using the possibilistic weighting scheme, the K-NNs of nontypical test samples [e.g., x in Fig. 8(b)] will have low weights. Consequently, the confidence values assigned to these samples will be low in both classes.

We should note here that several distance-based classifiers that can tolerate outliers (e.g., methods described in [34]) could be used to overcome the problem highlighted in Fig. 8. However, as mentioned earlier, our choice for the K-NN is motivated by the need for efficiency, interpretability of the results, and incremental learning.

C. Summarizing the Training Data

Theoretically, a K-NN classifier can achieve optimal results when the size of the training data goes to infinity. Unfortunately, large training data can slow down this classifier considerably and make it not practical for real-time applications, such as land mine detection. Another issue that needs to be addressed when designing a K-NN classifier is the potential bias of the output when the training data from the different classes are unbalanced. This problem arises in the land mine detection application as the number of clutter signatures is typically much larger than the number of mine signatures. To address these two main issues, we propose an approach that summarizes the training data by few representative prototypes. In the following, we first describe the extraction of the training alarms, then we outline our summarization process.

The training data consist of a set of alarms reported by the NUKEv6 prescreener and labeled as mines or false alarms using the ground truth. The prescreener reports the cross-track (x_s) and down-track (y_s) position (center of connected component) of each alarm s. As illustrated in Fig. 3, each alarm has around 300 depth values (depending on the position of ground bounce and the alignment). The mine signature is not expected to cover all the depth values. Typically, depending on the mine type and burial depth, the mine signature may extend over 30–80 depth values, i.e., it may cover no more than 10% of the extracted data cube. For example, in Fig. 3(b), the signature essentially extends from depth index 140 to depth index 200. There is little or no evidence that a mine is present in depth bins above or below this region. Thus, extracting one global EHD feature from the alarm may not discriminate between mine and clutter signatures effectively. To avoid this limitation, we extract the EHD feature from a small window with W_d=30 depth values. Since the ground truth for the depth value (z_s) is not provided, we visually inspect all training mine signatures and estimate this value. For the clutter signatures, this process is not trivial as clutter objects can have different characteristics and their signature can extend over a different number of samples. Instead, for each reported false alarm, we extract five equally spaced depths ($z_{s_1}, \ldots, z_{s_5}$) covering the entire depth range. Thus, each training signature s consists of a 30 (depth values) $\times$ 15 (scans) $\times$ 7 (channels) volume extracted from the aligned GPR data and centered at the identified alarm position (y_s, z_s).

The signatures within each class are expected to exhibit significant variations. For instance, clutter signatures can be caused by different types of buried objects. Similarly, mine signatures can have multiple subclasses corresponding to mines of different types and sizes, mines buried at different depths, different soil and weather conditions, etc.

To reduce the size of the training data without losing the within-class variations, we cluster the training samples into groups of homogeneous signatures. Each cluster would be represented by one representative signature. Only these representatives would be compared to the test signature to identify the K-NN. The number of selected representatives control the accuracy and efficiency of the classifier. A small number of representatives would make the classifier computationally more efficient (less signatures to compare), but less accurate (not enough prototypes to capture all variations within the training data). Ideally, the number of clusters should be decided by the real-time requirements of the complete system (e.g., vehicle speed, processing time of other system components).

Several clustering algorithms could be used to summarize the training samples. In the current implementation, we use the self-organizing feature maps (SOMs) [44]. Our choice is motivated by the fact that the SOM can represent the clusters by a map that

preserves the topology of the data. This is a desirable property that provides a simple and fast method to increase or decrease the number of representatives dynamically with a minimum impact on the classification accuracy. In particular, we use the SOM to cluster the mine and clutter signatures separately. For each class, we use a 10×10 map to identify 100 clusters. If, in operation mode, the system response is not fast enough, then the number of clusters could be reduced by subsampling the map of representatives (e.g., ignoring clusters at every other row and/or column).

We will refer to the clusters' representatives (R_i) as prototypes. We use R_i^M to denote the prototypes of the mine signatures and R_i^C to denote the prototypes of the clutter signatures. First, each training signature is assigned a fuzzy membership in the class of mines $\tilde{\mu}^M(y)$ and the class of clutter $\tilde{\mu}^C(y)$ using (4). Then, the memberships of the representative of cluster i are computed as the average of the memberships of all signatures assigned to cluster $\mathcal{C}_i$, i.e., the membership of R_i in the class of mines is computed using

$$\tilde{\mu}^M(R_i) = \frac{1}{\|\mathcal{C}_i\|} \sum_{y \in \mathcal{C}_i} \tilde{\mu}^M(y). \tag{8}$$

Similarly, the membership in the class of clutter is computed using

$$\tilde{\mu}^C(R_i) = \frac{1}{\|\mathcal{C}_i\|} \sum_{y \in \mathcal{C}_i} \tilde{\mu}^C(y) \tag{9}$$

where $\tilde{\mu}^M(y)$ and $\tilde{\mu}^C(y)$ are computed using (4).

D. Confidence Assignment

In testing, we cannot assume that the depth value is known. Thus, each potential target (identified by the prescreener) is tested at multiple depth values. We slide a $30 \times 15 \times 7$ window size along the depth axis with a 50% overlap between two consecutive signatures. A maximum of ten signatures are extracted for each target. For each signature, we extract the EHD as described in Section III-A, and use a possibilistic K-NN-based rule, as described in Section III-B.3, to assign a confidence value. First, for a given test signature S_T, we compute its distance to all representative prototypes. Then, we sort these distances and identify the K-NNs $S_T^1, \ldots, S_T^K$. The confidence value in the mine class is computed using

$$\mathrm{Conf}^M(S_T) = \frac{1}{K} \sum_{k=1}^{K} \tilde{\mu}^M(R_k) w^p(S_T, R_k). \tag{10}$$

Similarly, the confidence value in the clutter class is computed using

$$\mathrm{Conf}^C(S_T) = \frac{1}{K} \sum_{k=1}^{K} \tilde{\mu}^C(R_k) w^p(S_T, R_k). \tag{11}$$

In (10) and (11), $\tilde{\mu}^M(R_k)$ and $\tilde{\mu}^C(R_k)$ are the fuzzy memberships of prototype R_k in the mines and clutter classes, respectively, and $w^p(S_T, R_k)$ is the possibilistic weight defined in (7). Since $\tilde{\mu}^M$, $\tilde{\mu}^C$, and $w^p \in [0, 1]$, (10) and (11) generate confidence values in the range $[0, 1]$. The overall confidence of test signature S_T is computed using

$$\mathrm{Conf}(S_T) = \sqrt{\mathrm{Conf}^M(S_T) \times (1 - \mathrm{Conf}^C(S_T))}. \tag{12}$$

Since each target is tested at ten different depth values, we obtain ten confidence values. These values are combined using an order-weighted average (OWA) [45] to generate a single confidence value. An OWA operator [46] has a weight vector $\mathbf{W} = [w_1, \ldots, w_n]$ satisfying $\sum_{j=1}^{n} w_j = 1$, and aggregates the input vector $\mathbf{X} = [x_1, \ldots, x_n]$ using a function $F : \mathbb{R}^n \rightarrow \mathbb{R}$ and $F(X) = \sum_{j=1}^{n} w_j x_{(j)}$, where $x_{(j)}$ is the jth largest value of $\mathbf{X}$. The weight vector $\mathbf{W}$ is learned using the training data by minimizing the error function using the gradient descent [46].

TABLE I
STATISTICS OF THE DATASET

	Site A	Site B	Site C	Site D	Total
No. Collections	3	6	2	1	12
No. Mine Types	9	15	9	5	19
No. Mine Alarms	183	821	62	494	1560
No. Clutter Encounters	0	15	0	196	211
No. Clutter Alarms post prescreener	0	4	0	46	50
No. False Alarms detected by prescreener	426	1987	115	1350	3878
Area(m^2)	14813	15631	4054	7310	41808

IV. Experimental Setup

A. Dataset Statistics

The EHD-based detector was developed and tested with data collected using the NIITEK vehicle-mounted GPR system. The data were collected between November 2002 and July 2006 from four geographically distinct test sites. Sites A, B, and D are temperate climate test facilities with prepared soil and gravel lanes. Site C is an arid climate test facility with prepared soil lanes. The four sites have a total of 17 different lanes with known mine locations. All mines are antitank (AT) mines. In all, there are 19 distinct mine types that can be classified into three categories: AT metal (ATM), AT with low metal content (ATLM), and simulated mines (SIMs). The targets were buried up to 6 in deep. Multiple data collections were performed at each site at different dates, covering a ground area of 41 807.57 m^2, resulting in a large and diverse collection of mine and false alarm signatures. False alarms arise as a result of radar signals that present a mine-like character. Such signals are generally said to be a result of clutter. In this experiment, clutter arises from two different processes. One type of clutter is emplaced and surveyed in an effort to test the robustness of the algorithms. Other clutter results from human activity unrelated to the data collection or as a result of natural processes. We refer to this second kind of clutter as nonemplaced. Nonemplaced clutter includes objects discarded or lost by humans, soil inconsistencies and voids (due to formation processes, erosion, or excavation), stones, roots and other vegetation, as well as remnants of animal activity.

The statistics of the data are shown in Table I. The data collected from sites B and D have emplaced buried clutter. Although the lanes at sites A and C are prepared, they still contain nonemplaced clutter objects. Both metal and nonmetal nonemplaced clutter objects such as ploughshares, shell casings, and large rocks have been excavated from these sites. The emplaced

TABLE II
NUMBER OF METAL AND PLASTIC CASED MINES AND MINE SIMULANTS AND THEIR BURIAL DEPTHS

	Depth								Total
	-1"	0"	1"	2"	3"	4"	5"	6"	
Metal	12	37	124	68	151	34	119	77	777
Low-Metal	6	92	90	204	122	134	47	76	616
Simulants	48	0	20	47	23	29	0	0	167
Total	66	129	234	319	296	197	166	153	1560

clutter objects include steel scraps, bolts, soft-drink cans, concrete blocks, plastic bottles, wood blocks, and rocks. In all, there are 12 collections having 19 distinct mine types. Many of these mine types are present at several sites. The prescreener detected 1560 of the 1593 mines encountered in the data, yielding a 97.9% probability of detection (PD). Thus, only the detected 1560 mine signatures will be processed by the feature-based algorithms. The prescreener rejected 161 of 211 emplaced clutter objects encountered and yielded a total of 3828 false alarms associated with nonemplaced clutter objects. The number, type, and burial depth of the mines are given in Table II. As can be seen, the mines buried at 2.5 through 15.2 cm occupy 87.5% the total targets encountered versus 12.5% surface-laid or flush-buried mines.

B. Parameter Setting

The performance of the proposed EHD detector, and in particular the possibilistic K-NN depends on the values of K, m, and the parameters η_1 and η_2 used in (7). The value of m is simply fixed to 2, which is a common practice in this type of fuzzy and possibilistic membership functions. For the number of NNs considered, we experimented with several values of K. In general, the results improve as we increase K and values larger than 10 gave comparable results. Since larger values for K would require more computations, we fix K to 10.

The parameters η_1 and η_2 are learned from the training data. In particular, we identify the five nearest prototypes to each training sample, and we construct a histogram of all of these distances. Then, we set $\eta_1 = \mu_H$ and $\eta_2 = 3 \times \sigma_H$, where μ_H and σ_H are the mean and standard deviation of the histogram of distances. This choice ensures that during testing, prototypes within a distance of $\mu_H + 3 \times \sigma_H$ (computed using the training data) will be assigned a possibilistic membership higher than 0.5. The selection of this parameter is illustrated in Fig. 9.

C. Data Summarization

To speed up the K-NN classifier within the EHD detector, we summarize the training data by few representative prototypes, as described in Section III-C. Thus, for each cross-validation set, training alarms from 16 lanes would be first partitioned into mine and clutter alarms using the available ground truth. Then, the SOMs [44] would be used to cluster each group of signatures into a 10×10 map to identify the representative prototypes. Fig. 10 displays the SOM map of the mine prototypes for one of the 17 cross-validation sets. This map, which includes 100 mine prototypes, represents a summary of about 1300 mine signatures. For each prototype, we display its memberships in the mine and clutter classes. As can be seen, some of the prototypes

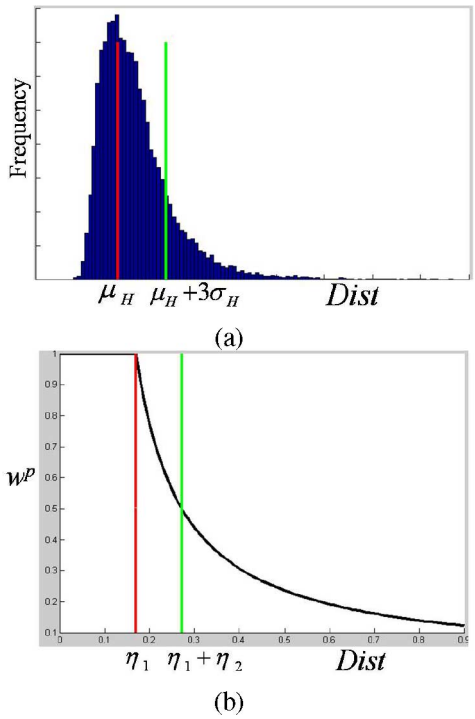

Fig. 9. Estimation of the possibilistic membership function parameters from the training data. (a) Histogram of the distances of the training data from the closest prototypes. μ_H and σ_H are the mean and standard deviation of this histogram. (b) Possibilistic membership function with parameters estimated in (a).

Fig. 10. SOM map of the mine prototype signatures for one training set.

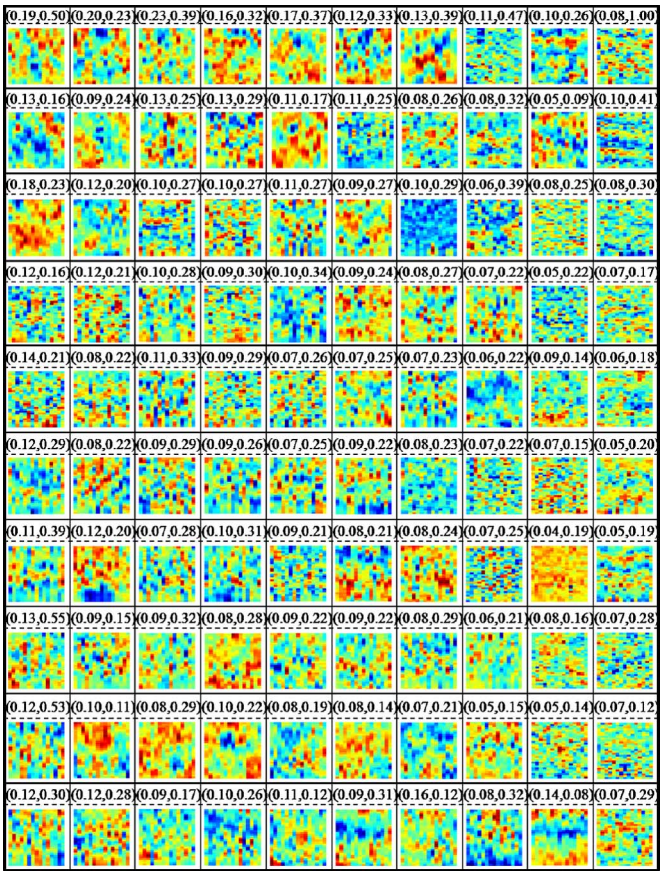

Fig. 11. SOM map of the clutter prototype signatures for one training set.

have strong and well-structured signatures. These prototypes, located in the top left corner of the map, have large membership in the class of mines (close to 1) and low membership in the clutter class (close to zero). There are also some prototypes that have weak signatures. These prototypes, located in the bottom right corner of the map, have smaller membership values in the mine class and larger memberships in the clutter class. Fig. 11 displays the SOM map of the clutter prototypes for the same cross-validation set. This map includes 100 prototypes and represents the summary of about 3000 clutter signatures. As can be seen, some of the clutter prototypes (e.g., top left corner) resemble the signatures of weak mine. These prototypes are assigned low membership values in the class of mines and would contribute to the overall confidence value [see (10)]. In other words, clutter signatures that have partial edge structure would be treated differently from clutter signatures that have high energy but no structure. Using this summarization, testing a new alarm would require computing and sorting 200 distances. The standard K-NN classifier would require computing and sorting over 4000 distances. If the K-NN classifier needs to run faster, the number of prototypes could be reduced by sampling the map. For instance, we could reduce the number to 25 by ignoring prototypes in every other column and every other row. Since adjacent prototypes are similar, this will not have a significant effect on the accuracy.

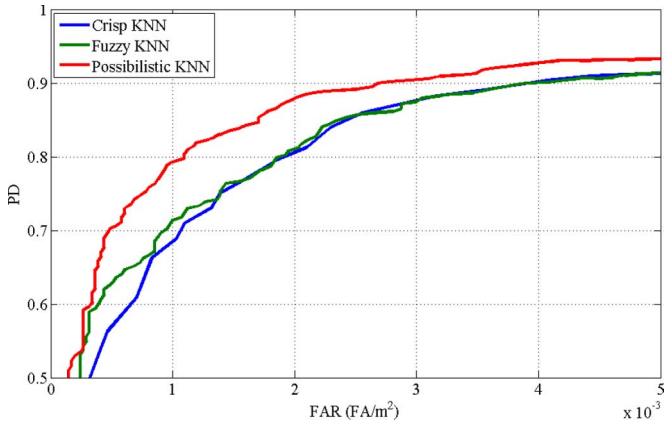

Fig. 12. Comparison of the performance of the possibilistic, fuzzy, and crisp K-NN classifiers.

D. Evaluation Method

To provide an objective and consistent evaluation of these algorithms, we use a testing/training unified framework (TUF) system. This system performs n-way cross-validation testing using lane-based cross-validation where each mine lane is, in turn, treated as a test set with the rest of the lanes used for training. The results of this process are scored using the mine detection assessment and scoring (MIDAS) system developed by the Institute for Defense Analysis [47]. The scoring is performed in terms of PD versus FAR. Confidence values are thresholded at different levels to produce ROC curve. For a given threshold, a mine is detected if there is an alarm within 0.25 m from the edge of the mine with confidence value above the threshold. Given a threshold, the PD is defined to be the number of mines detected divided by the number of mines. The FAR is defined as the number of false alarms per square meter.

E. Comparison of the Crisp, Fuzzy, and Possibilistic K-NN

To illustrate the advantages of the proposed possibilistic K-NN, we compare its performance to the crisp and fuzzy K-NN. For all methods, we use the same process to summarize the training data (since it is not practical to use the all of the training data). Fig. 12 compares the ROC curves for the three classifiers. As can be seen, the fuzzy K-NN is slightly better than the crisp K-NN at low FAR. This is due mainly to the fuzzy labels assigned to the clusters representatives and the weights assigned to the neighbors based on their relative distance from the test sample. The possibilistic K-NN has the best performance at all FAR values. In particular, for PD in the range of 70%–85%, the FAR is cut in half. This is due to the possibilistic weights assigned to the NNs. The distribution of the confidence values assigned to the mine and clutter signatures using the three classifiers is shown in Fig. 13. In each figure, the dotted line indicates the threshold that results in detecting 90% of the mines. As can be seen, the crisp K-NN tends to have binary confidence values. This is expected since the prototypes have crisp labels, and thus will be either counted as mines or clutter.

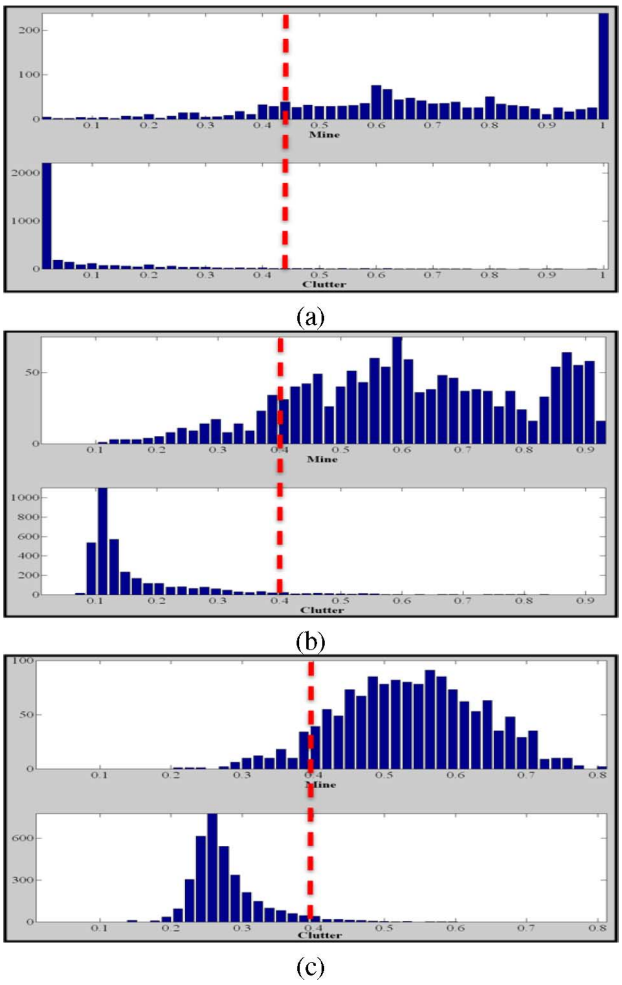

Fig. 13. Distribution of the confidence values assigned to the mine and clutter signatures using (a) crisp K-NN; (b) fuzzy K-NN; and (c) possibilistic K-NN.

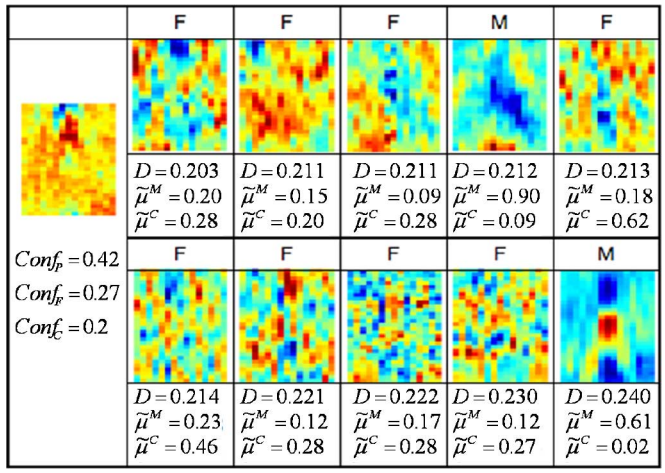

Fig. 14. Weak mine signature (left column) and its ten nearest prototypes. Conf_P, Conf_F, and Conf_C refer to the confidence values generated using the possibilistic, fuzzy, and crisp K-NN, respectively. For each prototype, we show its membership in the mine and clutter classes and its distance to the test signature.

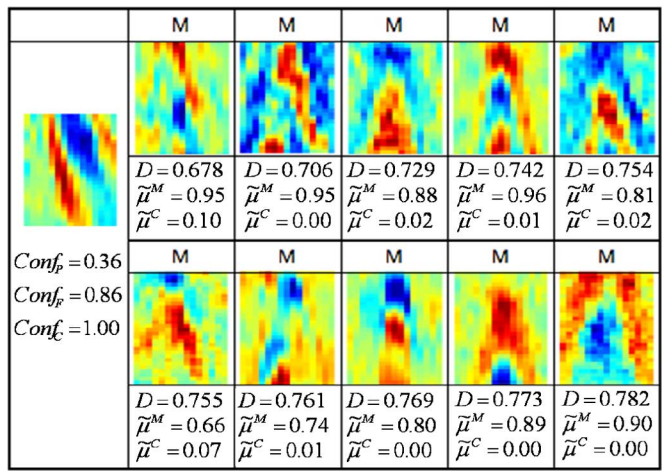

Fig. 15. Strong clutter signature (left column) and its ten nearest prototypes.

To analyze the results further, we select two signatures where the three classifiers differ significantly and display the intermediate results. Fig. 14 displays the signature of one weak mine (left column) and the ten nearest prototypes sorted by distance. For each prototype, we display its distance and its fuzzy membership in the mine and clutter classes. For this signature, the confidence values assigned by the possibilistic, fuzzy, and crisp classifiers are 0.42, 0.27, and 0.20, respectively. Thus, at the 90% PD, this signature will be detected by the possibilistic K-NN and missed by the fuzzy and crisp K-NN (refer to thresholds in Fig. 13). Only two of the ten nearest prototypes are mines. However, most of the other eight prototypes have features that resemble weak mines and have nonzero membership in the class of mines. This explains the reason why, for this test sample, the fuzzy K-NN outperforms the crisp K-NN (but both classifiers will not detect it at the 90% PD threshold). The possibilistic K-NN can detect this signature at the 90% PD threshold for two main reasons. First, distances of all ten nearest prototypes are small (compare these with the distances in Fig. 15). Thus, the possibilistic K-NN assigns high weights to all of them. The fuzzy K-NN, on the other hand, assigns relative weights. Thus, the last prototype, which is a mine, will get a much smaller weight. The second reason is that the proposed possibilistic combines confidence values assigned to both classes [refer to (12)]. Since the nearest clutter prototypes have low membership in the clutter class, the confidence in this class will be low. This, in turn, increases the overall confidence values.

Fig. 15 displays the signature of one strong clutter object and the ten nearest prototypes sorted by distance. This signature has high energy but it does not resemble typical mine signatures since it is missing the leading edge. The ten nearest prototypes are strong mines with a high membership degree in the class of mines. Thus, both the crisp and fuzzy K-NN assign a high confidence value to this signature. Using these classifiers, this signature will always be detected as a false alarm (even at 10% PD). The possibilistic K-NN, on the other hand, assigns a low confidence value, and this signature will not be a false alarm even at 90% PD. This is because all of the nearest prototypes are quite distant from the test signature, and thus, will be assigned very

low membership degrees. This, in turn, is due to the fact that the test signature is not a typical one in the training data, and is not represented by any of the prototypes (this is the scenario depicted in Fig. 8).

F. Comparison With Other Detectors

Several other algorithms were developed for the same NIITEK GPR data. In this section, we outline three distinct algorithms that were tested extensively and performed quite well. The performance of the proposed detector will be compared to these algorithms.

1) Hidden Markov Model Algorithm (HMM): The HMM algorithm [22], [24] treats the down-track dimension as the time variable and produces a confidence that a mine is present at various positions (x, y) on the surface being traversed. In particular, a sequence of observation vectors is produced for each point. These observation vectors encode the degree to which edges occur in the diagonal and antidiagonal directions. In particular, for every point (x_s, y_s), the strengths for the positive/negative diagonal/antidiagonal edges are computed. Then, the observation vector at a point (x_s, y_s) consists of a set of four features that encode the maximum edge magnitude over multiple depth values around (x_s, y_s). The HMM algorithm has a background and a mine model. Each model has three states and produces a probability value by backtracking through model states using the Viterbi algorithm. The probability value produced by the mine (background) model can be thought of as an estimate of the probability of the observation sequence given that there is a mine (background) present. The mine model is left to right model in which states are ordered and the transition probabilities for moving to a lower numbered state are zero.

2) Spectral Feature Algorithm (Spect): This detector aims at capturing the characteristics of a target in the frequency domain. It extracts the alarm spectral correlation feature (SCF) and formulates a confidence value based on similarity to prototypes that characterize mine objects [48]. The spectral features are derived from the energy density spectrum (EDS) of an alarm. The estimation of EDS involves three main steps: preprocessing, whitening, and averaging. Preprocessing estimates the ground level, aligns the data from each scan with respect to ground level, and removes the data above and near the ground surface. This step is needed to avoid an EDS that is dominated by the response of the ground bounce. The whitening step performs equalization on the spectrum from the background so that the estimated EDS reflects the actual spectral characteristics of an alarm. Averaging reduces the variance in the EDS.

3) Geometric Feature Algorithm (Geom): This detector is based on using geometric features as inputs to a single-hidden-layer feedforward OWA (FOWA) network [25], which is essentially a perceptron with a combination of scalar and OWA vector input features. An iterative technique that maximizes the area under the ROC curve is used to improve the accuracy of this algorithm [49]. The features presented to this network are geometric features captured at multiple-depth bins whitened version of the GPR data. In particular, we use the compactness, eccentricity, solidity, and area to filled area ratio. These features were based on the observation that the whitened energy signal for mines has a compact, solid, and circular shape in many of depth bins, while the signal for nonmine-like false alarms has an irregular shape.

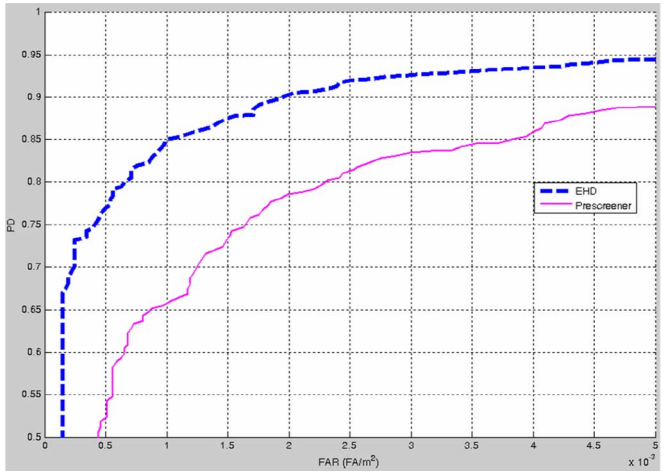

Fig. 16. Comparison of the EHD ROC curve with the prescreener ROC curve for the entire data collection.

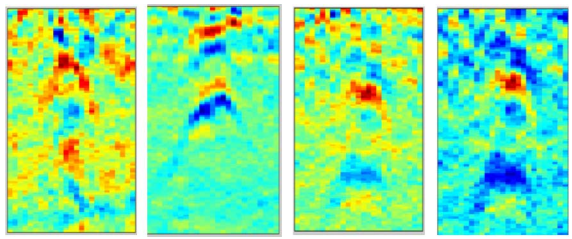

Fig. 17. Sample mine signatures where the EHD has increased the confidence values significantly.

G. Results

The alarms identified by the prescreener were used to train and test the EHD, HMM, Spect, and Geom detectors using lane-based cross-validation within the TUF environment. We should note here that all algorithms have been optimized by their authors using the same data collection. Fig. 16 compares the ROC curves for the confidence values generated by the prescreener with the one generated by the EHD detector. As can be seen, the EHD ROC curve is shifted left (i.e., lower FAR for the same PD) and shifted up (higher PD for the same FAR) when compared to the prescreener ROC. Thus, one can conclude that the EHD detector can discriminate between the mine and clutter signatures identified by the prescreener. Examination of the confidence values of individual alarms has indicated that the EHD has increased the confidence values of several "weak" mine signatures considerably. This behavior was illustrated and justified in Fig. 14. Fig. 17 displays more samples of these weak mine signatures. Similarly, the EHD has reduced the confidence values of several clutter signatures significantly. These are usually signatures with high energy content that do not have the coherent spatial edge distribution. This behavior was illustrated

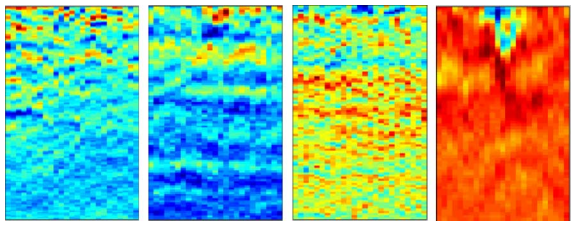

Fig. 18. Sample clutter signatures, identified by the prescreener, where the EHD has reduced the confidence values significantly.

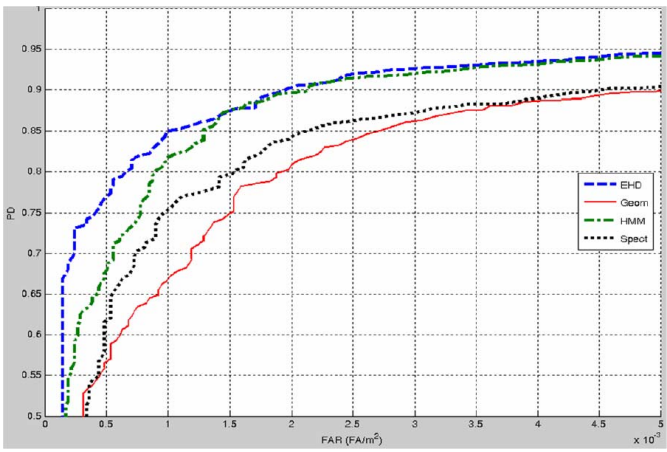

Fig. 19. Comparison of the ROC curves generated by the four detectors averaged over the alarms extracted from all sites.

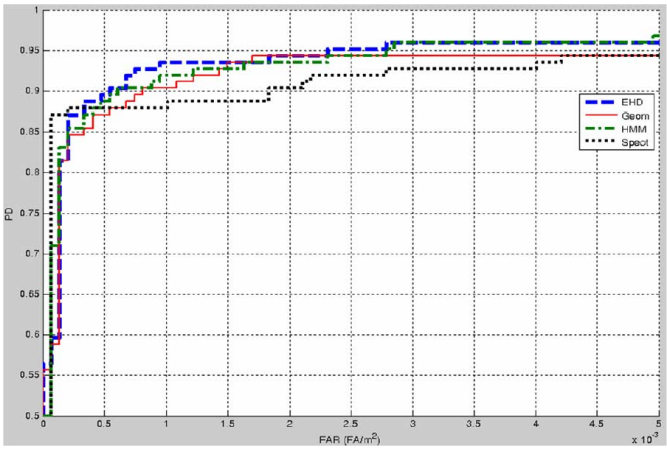

Fig. 20. Comparison of the ROC curves generated by the four detectors averaged over the alarms extracted from site A only.

and justified in Fig. 15. Fig. 18 displays more samples of these clutter signatures.

Fig. 19 displays the ROC curves associated with the EHD, HMM, Geom, and Spect detectors for all sites. The ROCs are displayed for the confidence values generated by each algorithm. As can be seen, the EHD detector has the best overall performance. However, this does not necessarily mean that the EHD detector outperforms the other algorithms for every alarm, or even for every site. To illustrate this point, we show the ROCs associated with each algorithm at each site in Figs. 20–23. As can be seen, sites A and C are relatively easier than sites B and D.

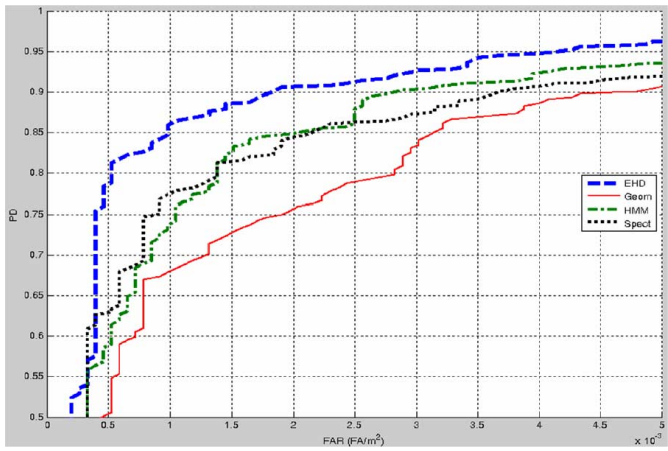

Fig. 21. Comparison of the ROC curves generated by the four detectors averaged over the alarms extracted from site B only.

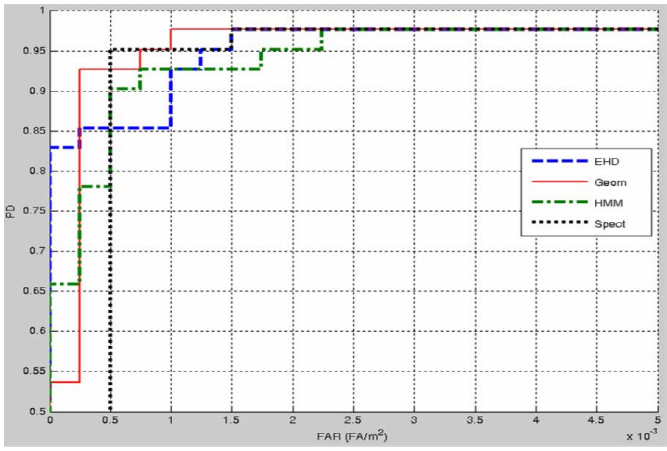

Fig. 22. Comparison of the ROC curves generated by the four detectors averaged over the alarms extracted from site C only.

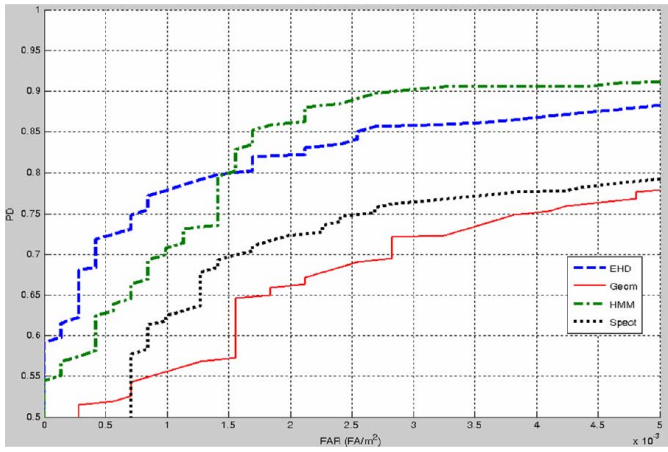

Fig. 23. Comparison of the ROC curves generated by the for detectors averaged over the alarms extracted from site D only.

This is partially due to the absence of clutter encounters in these collections. For these sites, all algorithms have a comparable good performance. Sites B and D include more alarms and some clutter objects. For these sites, the performance of the four

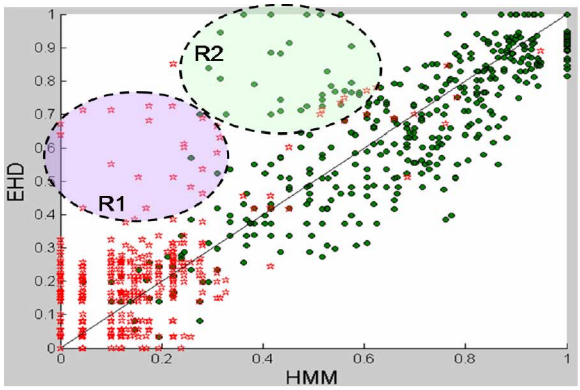

(a)

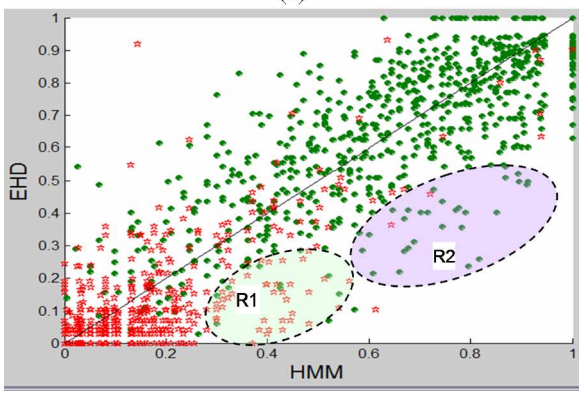

(b)

Fig. 24. Comparison of the EHD and HMM outputs for several mine (green dots) and clutter (red stars) signatures extracted from (a) subset of site A and (b) subset of site B.

detectors varies significantly. For site B, as shown in Fig. 21, the EHD detector is clearly the best detector. However, for site D, as shown in Fig. 23, the EHD detector has the best results for low PD (less than 80%), but the HMM detector is better at high PD. Furthermore, even within a small subset of the same site, the relative performance of different algorithms can vary significantly. For instance, in Fig. 24(a), the highlighted region (R1) includes mainly clutter signatures where the HMM algorithm outperforms the EHD (lower HMM confidence values). On the other hand, for the same subset, region (R2) includes mainly mine signatures where the EHD detector outperforms the HMM (higher EHD confidence). Fig. 24(b) highlights two other regions for alarms extracted from another site.

These results suggest that the output of these different algorithms could be fused to improve the overall performance. We are currently investigating different fusion techniques to achieve this goal [50], [51].

V. Conclusion

We have proposed an efficient and effective approach to discriminate between land mine and clutter signatures in GPR data. Our approach uses translation-invariant features, which are based on EHDs extracted from the 3-D GPR signatures, and a possibilistic K-NNs rule for confidence assignment. To speed up the classifier and reduce its sensitivity to atypical alarms, the training data are clustered and a small number of prototypes are identified. These prototypes capture signature variations due to differing soil conditions, mine types, weather conditions, and so forth. Moreover, fuzzy labels are assigned to these prototypes to reflect their degree of sharing among the mine and clutter classes. In addition to being simple and efficient, our approach is data-driven, and thus, could be easily retrained and adapted to data collected from other sites and/or with different GPR sensors.

The EHD algorithm outperformed all other algorithms involved in a large-scale cross-validation experiment that uses a diverse dataset that covers over 41 807 m^2 acquired from four outdoor test sites at different geographic locations over the course of several years. Many of the other algorithms have been described in earlier publications and are the result of several years of effort [22], [24], [25], [48], [49]. In addition, the EHD detector has been implemented and integrated in a land mine prototype system, has undergone extensive field testing, and has proved to be efficient and robust. Consequently, it has been implemented in real-time versions in vehicle-mounted GPR systems.

It is interesting to note that for the GPR sensor under consideration, the EHD is the only detector that uses fuzzy techniques to distinguish true detections from false alarms. Its better performance, as we have illustrated, is attributed to the fuzzy labels assigned to the prototypes and the possibilistic weights assigned to the K-nearest prototypes. The prototypes' fuzzy labels reflect their degree of sharing among the mine and clutter classes. These labels are very important in characterizing the ambiguity of weak mine and strong clutter signatures. The possibilistic weights indicate the typicality of the nearest prototypes and are helpful in rejecting atypical alarms that have strong energy. These experiments with extensive data on a real problem strongly support the possibilistic approach first proposed by Krishapuram and Keller [43].

Our analysis of the different detectors has indicated that the performance of these algorithms is strongly dependent upon a variety of factors that are not well understood. The factors appear to be somewhat correlated with geographical and environmental conditions but not strongly. These results suggest that the output of the different algorithms could be fused to improve the overall performance. We are currently investigating different fusion techniques to achieve this goal.

Acknowledgment

The authors would like to thank R. Harmon, R. Weaver, P. Howard, and T. Donzelli for their support of this study, E. Rosen and L. Ayers of the Institute for Defense Analyses (IDA) who provided much useful software and insight, L. Carin, L. Collins, and P. Torrione of Duke University and F. Clodfelter and others from NIITEK, Inc., for their technical discussion, insights, cooperation, discrimination algorithms, and GPR data. They would also like to thank the reviewers for their valuable comments. The views and conclusions contained in this document are those of the authors and should not be interpreted as representing the official policies, either expressed or implied,

of the Army Research Office, Office of Naval Research, Army Research Laboratory, or the U.S. Government.

REFERENCES

[1] "Hidden killers: The global landmine crisis," United States Department of State Report, Publication No. 10575, Sep. 1998.

[2] "Landmines: Demining News from the United Nations." U.N. Magazine, vol. 3.2, fourth quarter, 1998.

[3] J. A. MacDonald, *Alternatives for Landmine Detection*. Santa Monica, CA: RAND Corporation, 2003.

[4] J. N. Wilson, P. Gader, W. Lee, H. Frigui, and K. C. Ho, "A large-scale systematic evaluation of algorithms using ground-penetrating radar for landmine detection and discrimination," *IEEE Trans. Geosci. Remote Sens. E*, vol. 45, no. 8, pp. 2560–2572, Aug. 2007.

[5] S. L. Tantum, Y. Wei, V. S. Munshi, and L. M. Collins, "A comparison of algorithms for landmine detection and discrimination using ground penetrating radar," in *Proc. SPIE Conf. Detect. Remediation Technol. Mines Minelike Targets*, Orlando, FL, Apr. 2002, pp. 728–735.

[6] P. Gader, B. Nelson, H. Frigui, G. Vaillette, and J. Keller, "Fuzzy logic detection of landmines with ground penetrating radar," *Signal Process., Spec. Issue Fuzzy Logic Signal Process.*, vol. 80, no. 6, pp. 1069–1084, Jun. 2000.

[7] P. Torrione and L. Collins, "Application of Markov random fields to landmine detection in ground penetrating radar data," in *Proc. SPIE Conf. Detect. Remediation Technol. Mines Minelike Targets*, 2008, vol. 6953, pp. 69531B–69531B-12.

[8] T. R. Witten, "Present state of the art in ground-penetrating radars for mine detection," in *Proc. SPIE Conf. Detect. Remediation Technol. Mines Minelike Targets III*, Orlando, FL, 1998, vol. 3392, pp. 576–586.

[9] I. J. Won, D. A. Keiswetter, and T. H. Bell, "Electromagnetic induction spectroscopy for clearing landmines," *IEEE Trans. Geosci. Remote Sens. E*, vol. 39, no. 4, pp. 703–709, Apr. 2001.

[10] T. Nguyen, D. N. Hao, P. Lopez, F. Cremer, and H. Sahli, "Thermal infrared identification of buried landmines," in *Proc. SPIE Detect. Remediation. Technol. Mines Minelike Targets X*, 2005, vol. 5794, pp. 198–208.

[11] S. D. Somasundaram, K. Althoefer, J. A. S. Smith, and L. D. Seneviratne, "Detection of landmines using nuclear quadrupole resonance (NQR): Signal processing to aid classification," in *Climbing and Walking Robots*, G. V. M. O. Tokhi and M. Hossain, Eds. Heidelberg, Germany: Springer-Verlag, 2006, pp. 833–840.

[12] P. D. Gader, H. Frigui, B. Nelson, G. Vaillette, and J. M. Keller, "New results in fuzzy set based detection of landmines with gpr," in *Proc. Detect. Remediation Technol. Mines Minelike Targets IV*, Orlando, FL, 1999, vol. 3710, pp. 1075–1084.

[13] H. T. Kaskett and J. T. Broach, "Automatic mine detection algorithm using ground penetrating radar signatures," in *Proc. SPIE Conf. Detect. Remediation Technol. Mines Minelike Targets*, Orlando, FL, 1999, pp. 942–952.

[14] D. Carevic, "Clutter reduction and target detection in ground penetrating radar data using wavelets," in *Proc. SPIE Conf. Detect. Remediation Technol. Mines Minelike Targets IV*, Orlando, FL, 1999, pp. 973–978.

[15] D. Carevic, "Kalman filter-based approach to target detection and target-background separation in ground-penetrating radar data," in *Proc. SPIE Conf. Detect. Remediation Technol. Mines Minelike Targets IV*, Orlando, FL, Apr. 1999, pp. 1284–1288.

[16] A. Gunatilaka and B. A. Baertlein, "Subspace decomposition technique to improve GPR imaging of anti-personnel mines," in *Proc. SPIE Conf. Detect. Remediation Technol. Mines Minelike Targets V*, 2000, pp. 1008–1019.

[17] H. Brunzell, "Detection of shallowly burried objects using impulse radar," *IEEE Trans. Geosci. Remote Sens. E*, vol. 37, no. 2, pp. 875–886, Mar. 1999.

[18] O. Lopera, E. C. Slob, N. Milisavljevic, and S. Lambot, "Filtering soil surface and antenna effects from gpr data to enhance landmine detection," *IEEE Trans. Geosci. Remote Sens. E*, vol. 45, no. 3, pp. 707–717, Mar. 2007.

[19] S. Yu, R. K. Mehra, and T. R. Witten, "Automatic mine detection based on ground penetrating radar," in *Proc. SPIE Conf. Detect. Remediation Technol. Mines Minelike Targets IV*, Orlando, FL, Apr. 1999, vol. 3710, pp. 961–972.

[20] H. Frigui, K. satyanarayana, and P. Gader, "Detection of land mines using fuzzy and possibilistic membership functions," in *Proc. IEEE Conf. Fuzzy Syst.* May 25–28, 2003, vol. 2, pp. 834–839.

[21] H. Jui-feng and Z. Zheng-ou, "A new GPR targets feature extraction based on kernel method," in *Proc. Int. Conf. Signal Process. (ICSP)*, 31 Aug.–4 Sep. 2004, vol. 3, pp. 2159–2162.

[22] P. Gader, M. Mystkowski, and Y. Zhao, "Landmine detection with ground penetrating radar using hidden Markov models," *IEEE Trans. Geosci. Remote Sens. E*, vol. 39, no. 6, pp. 1231–1244, Jun. 2001.

[23] J. M. Stiles, P. Parra-Bocaranda, and A. Apte, "Detection of object symmetry using bistatic and polarimetric GPR observations," in *Proc. SPIE Conf. Detect. Remediation Technol. Mines Minelike Targets*, 1999, pp. 992–1002.

[24] H. Frigui, K. C. Ho, and P. Gader, "Real-time land mine detection with ground penetrating radar using discriminative and adaptive hidden markov models," *EURASIP J. Appl. Signal Process.*, vol. 12, no. 1, pp. 1867–1885, 2005.

[25] P. D. Gader, W.-H. Lee, and J. N. Wilson, "Detecting landmines with ground penetrating radar using feature-based rules order statistics, and adaptive whitening," *IEEE Trans. Geosci. Remote Sens. E*, vol. 42, no. 11, pp. 2522–2534, Nov. 2004.

[26] C. Yang and N. K. Bose, "Landmine detection and classification with complex-valued hybrid neural network using scattering parameters dataset," *IEEE Trans. Neural Netw.*, vol. 16, no. 3, pp. 743–753, May 2005.

[27] J. Zhang, Q. Liu, and B. Nath, "Landmine feature extraction and classification of GPR data based on SVM method," in *Proc. Int. Symp. Neural Netw.*, 2004, pp. 636–641.

[28] H. Frigui and P. Gader, "Detection and discrimination of landmines in ground-penetrating radar based on edge histogram descriptors," in *Proc. SPIE Conf. Detect. Remediation Technol. Mines Minelike Targets*, 2006, pp. 6217–6233.

[29] J. G. Proakis and D. G. Manolakis, *Digital Signal Processing*. Englewood Cliffs, NJ: Prentice-Hall, 1996.

[30] P. A. Torrione, C. S. Throckmorton, and L. M. Collins, "Performance of an adaptive feature-based processor for a wideband ground penetrating radar system," *IEEE Trans. Aerosp. Electron. Syst.*, vol. 42, no. 2, pp. 644–657, Apr. 2006.

[31] K. J. Hintz, "SNR improvements in NIITEK ground penetrating radar," in *Proc. SPIE Conf. Detect. Remediation Technol. Mines Minelike Targets IX*, Orlando, FL, Apr. 2004, pp. 399–408.

[32] M. Ohki and S. Hashiguchi, "Two-dimensional lms adaptive fileters," *IEEE Trans. Consum. Electron.*, vol. 37, no. 1, pp. 66–73, Feb. 1991.

[33] B. S. Manjunath, P. Salembier, and T. Sikora, *Introduction to MPEG 7: Multimedia Content Description Language*. New York: Wiley, 2002.

[34] D. M. Tax, "One-class classification," Ph.D. dissertation, TU Delft, Delft, The Netherlands, 2001.

[35] T. Hastie and R. Tibshirani, "Discriminant adaptive nearest neighbor classification and regression," in *Advances in Neural Information Processing Systems*, vol. 8, D. S. Touretzky, M. C. Mozer, and M. E. Hasselmo, Eds. Cambridge, MA: MIT Press, 1996, pp. 409–415.

[36] W. T. Chen, P. Gader, and H. Shi, "Lexicon-driven handwritten word recognition using optimal linear combinations of order statistics," *IEEE Trans. Pattern Anal. Mach. Intell.*, vol. 21, no. 1, pp. 77–82, Jan. 1999.

[37] T. Cover and P. E. Hart, "Nearest neighbor pattern classification," *IEEE Trans. Inf. Theory*, vol. IT-13, no. 1, pp. 21–27, Jan. 1967.

[38] S. A. Dudani, "The distance weighted k-nearest neighbor rule," *IEEE Trans. Syst., Man, Cybern.*, vol. SMC-6, no. 4, pp. 325–327, Apr. 1976.

[39] K. Hattori and M. Takahashi, "A new nearest neighbor rule in the pattem classification problem," *Pattern Recognit.*, vol. 32, no. 4, pp. 425–432, 1999.

[40] N. Zahid, O. Abouelala, M. Limouri, and A. Essaid, "Fuzzy clustering based on k-nearest-neighbours rule," *Fuzzy Sets Syst.*, vol. 120, no. 2, pp. 239–247, 2001.

[41] J. M. Keller, M. R. Gray, and J. A. Givens, "A fuzzy k-nearest neighbor algorithm," *IEEE Trans. Syst., Man, Cybern.*, vol. SMC-15, no. 4, pp. 580–585, Jul./Aug. 1985.

[42] D. Dubois and H. Prade, *Possibility Theory: An Approach to Computerized Processing of Uncertainty*. New York: Plenum, 1988.

[43] R. Krishnapuram and J. Keller, "A possibilistic approach to clustering," *IEEE Trans. Fuzzy Syst.*, vol. 1, no. 2, pp. 98–110, May 1993.

[44] T. Kohonen, *Self-Organization and Associative Memory*. Berlin, Germany: Springer-Verlag, 1989.

[45] P. Gader, R. Grandhi, W. Lee, J. Wislon, and D. Ho, "Feature analysis for the NIITEK ground-penetrating radar using order weighted averaging operators for landmine detection," in *SPIE Conf. Detect. Remediation Technol. Mines Minelike Targets*, Orlando, FL, Apr. 2004, vol. 5415, pp. 953–962.
[46] R. Yager and J. Kacprzyk, Eds., *The Ordered Weighted Averaging Operators: Theory and Applications*. Norwell, MA: Kluwer (Academic), 1997.
[47] L. Ayers and E. Rosen, "MIDAS: Mine detection assessment and scoring user's manual v1.1, institute for defense analysis," Tech. Rep., 2004.
[48] K. C. Ho, L. Carin, P. D. Gader, and J. N. Wilson, "An investigation of using the spectral characteristics from ground penetrating radar for landmine/clutter discrimination," *IEEE Trans. Geosci. Remote Sens. E*, vol. 46, no. 4, pp. 1177–1191, Apr. 2008.
[49] W.-H. Lee, P. D. Gader, and J. N. Wilson, "Optimizing the area under a receiver operating characteristic curve with application to landmine detection," *IEEE Trans. Geosci. Remote Sens. E*, vol. 45, no. 2, pp. 389–397, Feb. 2007.
[50] H. Frigui, L. Zhang, P. Gader, and D. Ho, "Context-dependent fusion for landmine detection with ground penetrating radar," in *Proc. SPIE Conf. Detect. Remediation Technol. Mines Minelike Targets IX*, 2007, vol. 6553, pp. 655321-1–655321-10.
[51] N. Milisavljevic and I. Bloch, "Possibilistic versus belief function fusion for antipersonnel mine detection," *IEEE Trans. Geosci. Remote Sens. E*, vol. 46, no. 5, pp. 1488–1498, May 2008.

Hichem Frigui (S'92–M'98) received the Ph.D. degree in computer engineering and computer science from the University of Missouri–Columbia, Columbia, in 1997.

From 1998 to 2004, he was an Assistant Professor at the University of Memphis. He is currently an Associate Professor and the Director of the Multimedia Research Laboratory, University of Louisville, Louisville, KY. His current research interests include research fields of fuzzy pattern recognition, data mining, and image processing with application to content-based multimedia retrieval and landmine detection. He is also involved in the development, testing, and real-time implementation of several land mine detection systems. He has authored or coauthored over 90 journals and refereed conference articles. He is an Associate Editor for the *Fuzzy Sets and Systems.*

Prof. Frigui was the recipient of the National Science Foundation Career Award for outstanding young scientists. He is currently an Associate Editor for the IEEE TRANSACTIONS ON FUZZY SYSTEMS.

Paul Gader (M'87–SM'99) received the Ph.D. degree in mathematics from the University of Florida, Gainesville, in 1986.

He was a Senior Research Scientist at Honeywell's Systems and Research Center, a Research Engineer and the Manager at the Environmental Research Institute of Michigan, and a Faculty Member at the University of Wisconsin–Oshkosh and the University of Missouri–Columbia. He is currently a Professor at the University of Florida. His current research interests include signal and image analysis, fuzzy systems, pattern recognition, and machine learning. He has led teams involved in real-time, handwritten address recognition systems for the U.S. Postal Service. He has led teams that devised and tested several real-time algorithms in the field for mine detection and is currently involved in a variety of land mine detection projects involving algorithm development for single and multisensor systems using ground-penetrating radars, electromagnetic induction sensors, electrooptic (EO)/IR imaging systems, and hyperspectral imaging sensors.